

Reachability-based Trajectory Safeguard (RTS): A Safe and Fast Reinforcement Learning Safety Layer for Continuous Control*

Yifei Simon Shao^{1,2}, Chen Chao², Shreyas Kousik¹, and Ram Vasudevan^{1,2}

Abstract—Reinforcement Learning (RL) algorithms have achieved remarkable performance in decision making and control tasks due to their ability to reason about long-term, cumulative reward using trial and error. However, during RL training, applying this trial-and-error approach to real-world robots operating in safety critical environment may lead to collisions. To address this challenge, this paper proposes a Reachability-based Trajectory Safeguard (RTS), which leverages trajectory parameterization and reachability analysis to ensure safety while a policy is being learned. This method ensures a robot with continuous action space can be trained from scratch safely in real-time. Importantly, this safety layer can still be applied after a policy has been learned. The efficacy of this method is illustrated on three nonlinear robot models, including a 12-D quadrotor drone, in simulation. By ensuring safety with RTS, this paper demonstrates that the proposed algorithm is not only safe, but can achieve a higher reward in a considerably shorter training time when compared to a non-safe counterpart.

I. INTRODUCTION

Reinforcement Learning (RL) is a powerful tool for automating decision making and control. For control in particular, multiple RL algorithms like Soft Actor Critic (SAC) [1] or Twin Delayed DDPG (TD3) [2] have been successfully applied to operate robots in simulation environments. RL is successful in this context due in part to its ability to construct a policy that describes how agents take actions to maximize long term cumulative reward.

Despite this utility, RL suffers from one critical shortcoming: its inability to make safety guarantees during learning or on a learned control policy. Even after applying an aggressive penalty for collision in a reward function, a trained agent may not be able to guarantee safety [3]. A variety of techniques have been applied to address this challenge which can be broadly categorized into three groups: policy update methods, model update methods, and shield methods. Next, we briefly summarize each of these categories.

Policy update methods focus on the challenge of conservatively updating a policy to maximize a reward function [4], [5]. This conservative policy update attempts to enforce constraints during training. However, these methods are only able to guarantee near constraint satisfaction. As a result,

This work is supported by the National Science Foundation Career Award #1751093, the Ford Motor Company via the Ford-UM Alliance under award N022977, and the Office of Naval Research under Award Number N00014-18-1-2575.

¹Mechanical Engineering, University of Michigan, Ann Arbor, MI. (syifei, skousik, ramv)@umich.edu

²Robotics Institute, University of Michigan, Ann Arbor, MI. joecc@umich.edu

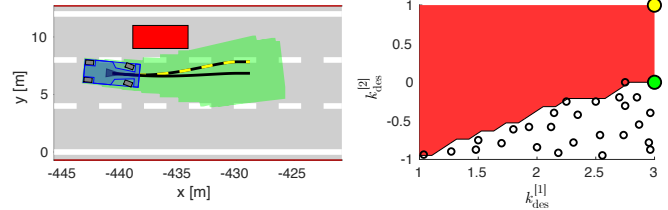


Fig. 1. An illustration of the proposed Reachability-based Trajectory Safeguard (RTS) enforcing safety during the training of a Reinforcement Learning (RL) policy. The RL policy selects a trajectory parameter (yellow and black circle on right) which corresponds to a trajectory plan (yellow and black dashed line on left) for the car (blue box on left). The plan is unsafe since the body of the car would collide with the obstacle (red box on left). RTS efficiently identifies that this choice of trajectory parameter is unsafe since it belongs to the unsafe trajectory parameter set (red set on right), which is computed via reachability analysis. To replace the RL agent’s plan with a new provably-safe one in real time, the parameter space is sampled (black circles), and the closest safe parameter (green) is selected as the new plan. Its trajectory (solid black on left) and corresponding forward reachable set (green, left) do not intersect the obstacle, guaranteeing safety when the car tracks the plan. By replacing the RL agent’s plan, RTS+RL enables the agent to learn from unsafe plans while the robot only executes safe plans.

these approaches typically can only qualitatively reduce the number of constraint violations, rather than guarantee safety.

Model update methods focus on improving the quality of a system dynamics model, then try to ensure the stability or safety of the learned model. To satisfy these stability/safety criteria, a variety of approaches have been developed. For instance, one can construct a stable policy that maximizes the region of attraction by creating a Lyapunov function at each time step [6]. On the other hand, one can construct a Control Barrier Function (CBF) to serve as a backup controller to safely guide model learning [7]. Similarly, one can use the Hamilton-Jacobi-Bellman (HJB) equation to identify a safety-preserving controller that can be applied near the boundary of the safe set while doing model learning via RL [8]. Finally, if one has a known control-invariant set, one can explore state space to improve a model until it is feasible to reach a goal state [9]. These techniques are powerful, but the challenge of constructing a Lyapunov function, CBF, solving the HJB equation, or having a known control-invariant set has restricted the complexity of models to which these techniques can be applied.

Finally, shield methods adjust a control policy at run-time using the knowledge they have about the systems dynamics to ensure safety. For instance, one can linearize a dynamic model and apply quadratic programming to ensure satisfaction of collision constraints [3]. Similarly, one can attempt to find a parameterized trajectory that satisfies constraints while trying to maximize a desirable behavior [10].

Unfortunately, applying these methods during real-time operation while making safety guarantees remains challenging. More recently, it has been shown how to adjust a control policy by selecting amongst a finite set of discrete actions [11]. In this formulation, a Forward Reachable Set (FRS) is constructed for each discrete action and used online to check for collisions to identify a safe action.

The present work develops a safety layer using a trajectory-parameterized reachable set, computed offline, over a continuous action space, to ensure safe learning online in real-time. This approach is motivated by Reachability-based Trajectory Design (RTD), a recent approach to safe robot motion planning, which uses an offline reachability computation and online receding horizon planning [12]. RTD uses a simplified, parameterized model to generate reference trajectories, or plans, and upper bounds the tracking error between the robot and planning model. Using the planning model and error, RTD finds an over-approximating FRS describing the location of the robot for each parameterized plan. The FRS then lets one identify unsafe plans and optimize over safe plans at runtime. However, RTD only optimizes trajectories over a short horizon, by assuming high-level planner has generated waypoints to be reached. In contrast, RL is able to optimize for a longer term reward.

This paper combines together the safety guarantees of RTD with the ability of RL to maximize long term cumulative reward. Hence, we propose Reachability based Trajectory Safeguard (RTS) for RL. RTS includes a safety layer that can be used for both *training* and *at runtime*. We let the RL agent choose *trajectory parameters* in continuous space instead of control inputs. This (1) lets us leverage reachability analysis to ensure entire trajectories are safe, and (2) reduces the dimension of the RL agent’s action space, speeding up runtime operation. Critically, RTS+RL enables safe training and testing despite for a model-free RL agent.

We demonstrate our method on three different nonlinear systems: a 4-D cartpole swing up task on a limited track, a 5-D car on an obstacle course, and a 12-D quadrotor drone in a cluttered tunnel. On all three systems, RTS+RL achieves collision-free training and evaluation while outperforming a baseline RL agent in terms of cumulative reward and shorter training time. That is, RTS+RL safely completes more tasks with fewer training episodes.

A. Contributions

The contributions of this work are three-fold. First, we propose the RTS algorithm for safe, real-time RL training and deployment using a continuous action space. Second, we reduce the conservatism of RTD’s reachable sets with a novel tracking error representation. Third, we demonstrate the capability of RTS+RL on a cartpole robot, a car, and a quadrotor in simulation.

The remainder of the paper is organized as follows. In Sec. II, we model the robot and the environment. In Sec. III, we compute reachable sets of the robot offline. In Sec. IV, we use the reachable sets online (during training) to ensure

safety. In Sec. V, we demonstrate the method on three robots. Finally, Sec. VI provides concluding remarks.

B. Notation

Points, vectors, and point/vector-valued functions (resp. sets, arrays, and set/array-valued functions) are in lowercase (resp. uppercase) italics. The real numbers are \mathbb{R} ; the natural numbers are \mathbb{N} . For $n, m \in \mathbb{N}$, we let $\mathbb{N}_n = \{1, 2, \dots, n\} \subset \mathbb{N}$, and $\mathbb{N}_n + m = \{1 + m, \dots, n + m\}$. The n -dimensional special orthogonal group is $\text{SO}(n)$. Let A be a set. Its power set is $\text{pow}(A)$, and its cardinality is $|A|$. If A is indexed by elements of a set B , we write $a^{(b)} \in A$ for $b \in B$.

Brackets denote concatenation when the size of vectors/matrices are important; e.g., if $v_1, v_2 \in \mathbb{R}^n$, then $[v_1, v_2] \in \mathbb{R}^{n \times 2}$ and $[v_1^\top, v_2^\top]^\top \in \mathbb{R}^{2n}$. Otherwise, we write $(v_1, v_2) \in \mathbb{R}^{2n}$. We use $\text{diag}(v_1, v_2, \dots, v_n)$ to place the elements of each input vector (in order) on the diagonal of a matrix with zeros elsewhere. We denote an empty vector/matrix as $[\]$.

We index elements of vectors and matrices as follows. Denote a multi-index as $I = \{i_1 < i_2 < \dots < i_p\} \subset \mathbb{N}_n$ with $i_p \leq n$, $p \leq n$, and $|I| = p$. If $v \in \mathbb{R}^n$, $v^{[I]} \in \mathbb{R}^p$ contains the elements of v indexed by I . Let $M \in \mathbb{R}^{n \times m}$ be a matrix; let $I_1 \subset \mathbb{N}_n$, and $I_2 \subset \mathbb{N}_m$, with $|I_1| = p \leq n$ and $|I_2| = q \leq m$. Then $M^{[I_1, I_2]}$ is a $p \times q$ sub-matrix of M with the elements indexed by I_1 (for the rows) and I_2 (for the columns). Similarly, $M^{[:, I_2]}$ is the $n \times q$ sub-matrix of the columns of M indexed by I_2 . If $M^{(i)}$ is the i^{th} matrix in a set, $[M^{(i)}]^{[j]}$ is its j^{th} element.

Let $\text{box}(c, l, R) \subset \mathbb{R}^n$ be a *rotated box*, with center $c \in \mathbb{R}^n$, edge lengths $l \in \mathbb{R}^n$, and rotation $R \in \text{SO}(n)$:

$$\text{box}(c, l, R) = c + R \cdot \left([-l^{[1]}, l^{[1]}] \times \dots \times [-l^{[n]}, l^{[n]}] \right). \quad (1)$$

If $R = 0$, we say the box is an *axis-aligned box*.

II. ROBOT AND ENVIRONMENT

This section describes the robot and its surroundings.

A. Modeling the Robot

1) *High Fidelity Model*: We express the robot’s motion using a *high-fidelity model*, $f : X \times U \rightarrow \mathbb{R}^{n_x}$, with state space $X \subset \mathbb{R}^{n_x}$, control input space $U \subset \mathbb{R}^{n_u}$, and

$$\dot{x}(t) = f(x(t), u), \quad (2)$$

where $t \in T = [0, t_{\text{fin}}]$ is time in each receding-horizon planning iteration, $x : T \rightarrow \mathbb{R}^{n_x}$ is a trajectory of the high-fidelity model, and $u \in U$ is the control input. We require that f is Lipschitz continuous, and that T , X , and U are compact, so trajectories of the model exist. We assume the high-fidelity model accurately describes the robot’s dynamics.

Our goal is to represent rigid-body robots moving through space, so we require that the robot’s state $x \in X$ includes the robot’s position p in a *position subspace* $P \subset \mathbb{R}^{n_p}$ ($n_p = 1, 2$, or 3). In particular, this is the robot’s center of mass or baselink position in a global coordinate frame. We use a projection operator $\text{proj}_P : X \rightarrow P$ to get the robot’s position from a state $x \in X$ as $p = \text{proj}_P(x)$.

2) *Planning Model*: Our receding-horizon planning framework, necessitates fast, frequent replanning for real-time operation; doing so is typically challenging with a high-fidelity model directly, so we use a simpler planning model and bound the resulting error. Let $K \subset \mathbb{R}^{n_K}$ denote a compact space of *trajectory parameters* (detailed below). The *planning model* is a map $p_{\text{plan}} : T \times K \rightarrow P$ such that

- 1) p_{plan} is smooth almost everywhere $t \in T$ and $k \in K$,
- 2) $p_{\text{plan}}(0, k) = 0$ for all $k \in K$, and
- 3) $\dot{p}_{\text{plan}}(t_{\text{fin}}, k) = 0$ for all $k \in K$.

A single trajectory $p_{\text{plan}}(\cdot, k) : T \rightarrow P$ is referred to as a *plan*. Note, every plan begins at $t = 0$ without loss of generality (WLOG), and every plan is of duration t_{fin} . We use the smoothness of p_{plan} to compute reachable sets in Section III. We fix $p_{\text{plan}}(0, k) = 0$ arbitrarily because we can translate/rotate any plan to the position/orientation of the high-fidelity model at the beginning of each planning iteration. We fix $\dot{p}_{\text{plan}}(t_{\text{fin}}, \cdot) = 0$ so all plans end with a braking *failsafe maneuver*. If the robot fails to find a safe plan in a planning iteration, it can continue a previously-found safe plan, enabling persistent safety [12, Thm. 39].

3) *The Trajectory Parameter Space*: We require that K is an axis-aligned, box-shaped set. Let $c_K, \Delta_K \in \mathbb{R}^{n_K}$. Then

$$K = \text{box}(c_K, \Delta_K, 0). \quad (3)$$

We also break the parameter space into two parts, so that $K = K_{\text{init}} \times K_{\text{des}}$. Denote $k = (k_{\text{init}}, k_{\text{des}}) \in K$.

The first part, K_{init} , determines a plan's initial velocity, $\dot{p}_{\text{plan}}(0, k_{\text{init}})$; this ensures one can choose a plan that begins at the same velocity as the robot. To this end, we define an *initial condition function*, $f_{\text{init}} : X \rightarrow K_{\text{init}}$, for which $x \mapsto k_{\text{init}}$. Suppose the robot is at a state x and applying a control input u . We implement f_{init} by setting $\dot{p}_{\text{plan}}(0, k) = \text{proj}_P(f(x, u))$ and solving for k_{init} , where we have abused notation to let proj_P project the relevant coordinates.

The second part, K_{des} , specifies positions or velocities reached by a plan during $(0, t_{\text{fin}}] \subset T$. So, instead of choosing control inputs, the RL agent chooses k_{des} in each receding-horizon planning iteration. This design choice is an important feature of RTS+RL, because we can design a tracking controller (discussed below) to obtain stability guarantees and obey actuator limits, and let RL focus on decision making. Note, different choices of k_{des} may be safe or unsafe, whereas k_{init} is determined by the robot's state at $t = 0$.

4) *Receding-horizon Timing*: We specify the rate of receding-horizon planning with a *planning time*, $t_{\text{plan}} \in (0, t_{\text{fin}})$. In each planning iteration, if a new, safe plan is found before t_{plan} , the robot begins tracking it at t_{plan} . Otherwise, the robot continues its previous plan. We determine the robot's initial condition x_0 in each planning iteration by forward-integrating the high-fidelity model for the duration t_{plan} while the robot is tracking its previous plan.

5) *Tracking Controller and Error*: We generate control inputs with a *tracking controller*, $u_{\text{trk}} : T \times X \times K \rightarrow U$, which attempts to minimize the *tracking error* between the high-fidelity model state and a plan. We define the *tracking error*

as a trajectory $e : T \rightarrow \mathbb{R}^{n_P}$ for which

$$e(t; x_0, k) = p(t; x_0, k) - p_{\text{plan}}(t, k) \quad \text{and} \quad (4)$$

$$x(t; k, x_0) = \int_0^t f(x(s), u_{\text{trk}}(t, x(s), k)) ds + x_0, \quad (5)$$

where $x_0 \in X$ such that $p(0; x_0, k) = 0$ and $\dot{p}_{\text{plan}}(0; k) = \dot{p}(0)$, with $p(\cdot) = \text{proj}_P(x(\cdot))$. Note, e is bounded because f is Lipschitz and T , U , and K are compact. We account for tracking error to ensure safety in Sec. III and IV.

B. Modeling the Robot's Environment

1) *Forward Occupancy*: The position coordinate $p \in P$ typically describes the motion of the robot's center of mass, but we require the robot's entire body to avoid obstacles. So, we define the *forward occupancy map* $\text{FO} : X \rightarrow \text{pow}(P)$, for which $\text{FO}(x) \subset P$ is the volume occupied by the robot at state $x \in X$. Since we only consider rigid body robots in this work, we conflate the robot's workspace with P . Note this work can extend to non-rigid robots such as multilink arms [13].

2) *Safety and Obstacles*: We define *safety* as collision avoidance. Let an *obstacle* $O \subset P$ be a region of workspace for which, if the robot is at a state x and $\text{FO}(x) \cap O \neq \emptyset$, the robot is *in collision*. We assume each obstacle is a box, $O = \text{box}(c, l, R) \subset P$, and static with respect to time; note that typical mapping and perception algorithms output rotated boxes [14], [15]. We also assume that the robot need only avoid a finite number of obstacles for any plan. We assume the robot can sense every obstacle instantaneously within a finite distance d_{sense} of its position, as in [12, Thm. 39]. Note, d_{sense} is lower-bounded based on the robot's maximum speed, which exists because X and U are compact.

III. OFFLINE REACHABILITY ANALYSIS

Offline, we compute a Planning Reachable Set (PRS), $\mathcal{R}_{\text{plan}}$, of the planning model, then bound tracking error with an Error Reachable Set (ERS), \mathcal{R}_{err} . Online, we use the PRS and ERS to build safety constraints (in the next section).

A. Planning Reachable Set

We represent the PRS with zonotopes using an open-source toolbox called CORA [16]. A zonotope is a set

$$\mathcal{Z}(c, G) = \{y \in \mathbb{R}^n \mid y = c + G\beta, \beta \in [-1, 1]^m\}, \quad (6)$$

where $c \in \mathbb{R}^n$ is the zonotope's *center*, $G \subset \mathbb{R}^{n \times m}$ is a *generator matrix*, and β is a *coefficient vector*. Points in the zonotope are a linear combination of c with columns of G , also called the *generators* of the zonotope.

1) *PRS Computation Setup*: We provide the toolbox [16] with three inputs to compute the PRS. First, we partition T into $m_T \in \mathbb{N}$ intervals. Let $\Delta_T = t_{\text{fin}}/m_T$, $T^{(1)} = [0, \Delta_T]$, and $T^{(i)} = ((i-1) \cdot \Delta_T, i \cdot \Delta_T]$. Then,

$$T = \bigcup_{i=1}^{m_T} T^{(i)}. \quad (7)$$

Second, we provide an augmented state $z = (p, k)$ with $\dot{z} = (\dot{p}_{\text{plan}}, 0)$. Third, since all plans begin at $p_{\text{plan}}(0, \cdot) = 0$, we

provide an initial condition set as a zonotope $Z_{\text{plan}}^{(0)} \subset P \times K$, with center $c^{(0)} = (0_{n_P \times 1}, c_K) \in \mathbb{R}^m$ and generator matrix $G^{(0)} = \text{diag}(0_{n_P \times 1}, \Delta_K) \in \mathbb{R}^{m \times m}$, where $m = n_P + n_K$.

2) *PRS Representation*: The PRS is represented as

$$\mathcal{R}_{\text{plan}} = \left\{ Z_{\text{plan}}^{(i)} = \mathcal{Z}\left(c_{\text{plan}}^{(i)}, G_{\text{plan}}^{(i)}\right) \subset P \times K \mid i \in \mathbb{N}_{m_T} \right\}, \quad (8)$$

which conservatively contains all plans and parameters: if $t \in T^{(i)}$ and $k \in K$, then $(p_{\text{plan}}(t, k), k) \in Z_{\text{plan}}^{(i)}$ [17, Thm 6.6].

3) *Trajectory Parameter Partition*: We find in practice that the conservatism of the PRS zonotope representation is proportional to the size of K_{init} . So, we partition K_{init} into $m_K \in \mathbb{N}$ axis-aligned boxes $K_{\text{init}}^{(j)} \subset K$ such that

$$K \subseteq \bigcup_{j=1}^{m_K} (K_{\text{init}}^{(j)} \times K_{\text{des}}) \quad (9)$$

and $K_{\text{init}}^{(i)} \cap K_{\text{init}}^{(j)} = \emptyset$ when $i \neq j$. We compute (8) for each $K^{(j)} = K_{\text{init}}^{(j)} \times K_{\text{des}}$, and choose which PRS to use online (in each planning iteration) based on the robot's initial condition, by choosing j such that $f_{\text{init}}(x_0) \in K_{\text{init}}^{(j)}$.

B. Error Reachable Set

The ERS bounds tracking error as in (4). Novel to this work, we also use the ERS to bound the robot's forward occupancy in workspace, whereas [17], [18] bounded the occupancy in the PRS, which is more conservative in practice.

1) *Initial Condition Partition*: Notice that tracking error depends on the robot's initial condition $x_0 \in X_0 = \{x_0 \in X \mid \text{proj}_P(x_0) = 0\}$. Just as we partitioned K_{init} to reduce PRS conservatism, we partition X_0 to reduce ERS conservatism. We choose $m_0 \in \mathbb{N}$ axis-aligned boxes $X_0^{(h)}$ such that

$$X_0 \subseteq \bigcup_{h=1}^{m_0} X_0^{(h)}, \quad (10)$$

and $X_0^{(i)} \cap X_0^{(j)} = \emptyset$ when $i \neq j$.

2) *Zonotope ERS*: With our partition of X_0 , we represent the ERS as a collection of zonotopes

$$\mathcal{R}_{\text{err}} = \{Z_{\text{err}}^{(i,j,h)} \subset P \mid (i, j, h) \in \mathbb{N}_{m_T} \times \mathbb{N}_{m_K} \times \mathbb{N}_{m_0}\} \quad (11)$$

for which, if $t \in T^{(i)}$, $k = (k_{\text{init}}, k_{\text{des}}) \in K^{(j)}$, $x_0 \in X_0^{(h)}$, and $f_{\text{init}}(x_0) = k_{\text{init}}$, then

$$\text{FO}(x(t; k, x_0)) \subseteq \{p_{\text{plan}}(t, k)\} + Z_{\text{err}}^{(i,j,h)} \quad (12)$$

with x as in (5) and $+$ denoting set addition [13, Lem. 6].

3) *Computing the ERS via Sampling*: It is often challenging to compute (11) using reachability tools such as [16] due to the high-dimensional, nonlinear tracking error. Instead, we use the following sampling-based approach, which modifies [17, Alg. 3] to include forward occupancy. Our goal is to conservatively estimate worst-case tracking error using a finite number of samples in $K^{(j)} \times X_0^{(h)}$.

We create samples using the axis-aligned box structure of $K^{(j)}$ and $X_0^{(h)}$. An axis-aligned box $B \subset \mathbb{R}^n$ can be expressed $[-l_1, l_1] \times \dots \times [-l_n, l_n]$. We call the set $\{-l_1, l_1\} \times \dots \times$

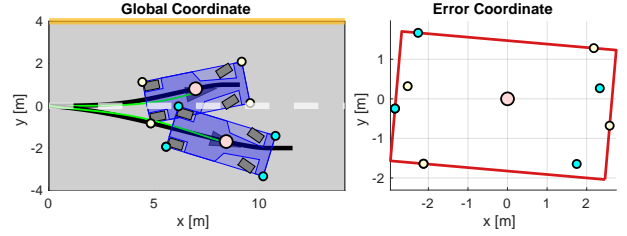


Fig. 2. To compute the maximum tracking error for the two sampled plans together at the sampled time instant below, we use the high fidelity model to track each plan (black). The tracking errors (yellow, cyan) are shown on the right with respect to the robot's center of mass (pink) for one sampled time instant in error coordinate. We bound the error using a minimum area rotated rectangle (red), and call that the max tracking error for the two sampled trajectories

$\{-l_n, l_n\}$ the corners of B . Let $C^{(j,h)}$ denote the corners of $K^{(j)} \times X_0^{(h)}$. We use each element of each $C^{(j,h)}$ as a sample.

Using all of the samples $(k, x_0) \in C^{(j,h)}$, we find the zonotope $Z_{\text{err}}^{(i,j,h)}$ as follows. First, if needed, we adjust k_{init} such that $f_{\text{init}}(x_0) = k_{\text{init}}$. Then, we find x as in (5) and

$$V^{(i,j,h)} = \bigcup_{(t,k,x_0) \in S} \text{FO}(x(t; k, x_0)) - \{p_{\text{plan}}(t, k)\}, \quad (13)$$

with $S = T^{(i)} \times C^{(j,h)}$ and $-$ denoting set subtraction. Note, in practice, we discretize $T^{(i)}$ to estimate this union, and numerically estimate x with a standard differential equation solver. Finally, we compute each ERS zonotope as

$$Z_{\text{err}}^{(i,j,h)} = \text{minBoundingBox}(V^{(i,j,h)}), \quad (14)$$

where minBoundingBox returns a minimum bounding box using [19]. Note, $\text{box}(c, l, R) = \mathcal{Z}(c, R \text{diag}(l))$ by (6). A toy example of (14) is shown in Fig. 2.

In an improvement over proofs in [17], we justify why our ERS computation approach can satisfy (12) in the supplementary material. Next, we use the PRS and ERS to enforce safety at runtime.

IV. ONLINE SAFE REINFORCEMENT LEARNING

This section describes RTS+RL's online training and testing, wherein the robot only chooses safe plans while *still learning from unsafe plans*. The main result is in Thm. 2.

To enforce safety, we combine the PRS (i.e., all plans) and ERS (i.e. tracking error) to build a Forward Reachable Set (FRS) containing the motion of the high-fidelity model tracking any plan. If a subset of the FRS corresponding to a plan is collision free, then that plan is safe.

A. Reachability-based Trajectory Safeguard (RTS)

Consider a single planning iteration. Suppose the robot is generating a plan beginning from an initial condition $x_0 \in X$. We present all computations from here on in the robot's local coordinate frame at $t = 0$, so $\text{proj}_P(x_0) = 0$. We build the FRS, use it to create safety constraints, then present an algorithm to ensure the robot only chooses safe plans.

Before we construct the FRS, we choose the PRS and ERS zonotopes from the partition of K and X_0 . Pick $x_0 \in X_0^{(h)}$ and $K^{(j)}$ such that if $k_{\text{init}} = f_{\text{init}}(x_0)$, then $k = (k_{\text{init}}, d_{\text{des}}) \in K^{(j)}$. Let $i \in \mathbb{N}_{m_T}$ (i.e., the time interval $T^{(i)}$) be arbitrary. For the rest of this section, we consider the zonotopes

$$Z_{\text{plan}}^{(i,j)} = \mathcal{Z}\left(c_{\text{plan}}^{(i,j)}, G_{\text{plan}}^{(i,j)}\right) \subset P \times K \text{ and} \quad (15)$$

$$Z_{\text{err}}^{(i,j,h)} = \mathcal{Z}\left(c_{\text{err}}^{(i,j,h)}, G_{\text{err}}^{(i,j,h)}\right) \subset P. \quad (16)$$

1) *FRS Construction*: We represent the FRS as zonotopes $Z_{\text{FRS}}^{(i,j,h)} \subset P \times K$ built from the PRS and ERS zonotopes:

$$Z_{\text{FRS}}^{(i,j,h)} = \mathcal{Z}\left(c_{\text{plan}}^{(i,j)} + \begin{bmatrix} c_{\text{err}}^{(i,j,h)} \\ 0_{n_K \times 1} \end{bmatrix}, \begin{bmatrix} G_{\text{plan}}^{(i,j)} \\ G_{\text{err}}^{(i,j,h)} \end{bmatrix}\right), \quad (17)$$

which follows from the zonotope Minkowski sum [20]. Note, the first n_P rows of $G_{\text{plan}}^{(i,j)}$ correspond to all n_P rows of $G_{\text{err}}^{(i,j,h)}$ (and similarly for the centers).

2) *Creating Safety Constraints*: Let $\{O^{(m)}\}_{m=1}^{n_{\text{obs}}}$ be the set of obstacles that the robot must avoid in the current planning iteration. The robot must choose k_{des} such that, if $k = (k_{\text{init}}, k_{\text{des}})$, then $\text{FO}(x(t; x_0, k)) \cap O^{(m)} = \emptyset \forall m$. To check this intersection, we introduce *slicing*. Let $c \in \mathbb{R}^n, G \in \mathbb{R}^{n \times p}$. Let $I \subseteq \mathbb{N}_p$ be a multi-index and $\beta \in [-1, 1]^{|I|}$. We define

$$\text{slice}(\mathcal{Z}(c, G), I, \beta) = \mathcal{Z}\left(c + G^{[I, I]} \beta, G^{[:, \mathbb{N}_p \setminus I]}\right). \quad (18)$$

From (6), a sliced zonotope is a subset of the original zonotope. We use slicing to identify unsafe plans:

Lemma 1. Consider the obstacle $O^{(m)} = \mathcal{Z}\left(c_{\text{obs}}^{(m)}, G_{\text{obs}}^{(m)}\right) \subset P$ and denote $Z_{\text{FRS}}^{(i,j,h)} = \mathcal{Z}\left(c_{\text{FRS}}^{(i,j,h)}, G_{\text{FRS}}^{(i,j,h)}\right)$. Suppose $G_{\text{FRS}}^{(i,j,h)}$ has $n \in \mathbb{N}$ generators. Let $I = \mathbb{N}_{n_K} + n_P$. Denote

$$G_{\text{slc}}^{(i,j,h)} = [G_{\text{FRS}}^{(i,j,h)}]^{[\mathbb{N}_{n_P}, I]}, \quad (19)$$

$$G_{\text{extra}}^{(i,j,h)} = [G_{\text{FRS}}^{(i,j,h)}]^{[\mathbb{N}_{n_P}, \mathbb{N}_n \setminus I]}, \quad (20)$$

$$Z_{\text{slc}}^{(i,j,h)} = \mathcal{Z}\left(c_{\text{FRS}}^{(i,j,h)}, G_{\text{slc}}^{(i,j,h)}\right) \text{ and} \quad (21)$$

$$Z_{\text{extra}}^{(i,j,h)} = \mathcal{Z}\left(0, G_{\text{extra}}^{(i,j,h)}\right). \quad (22)$$

Let $k = (k_{\text{init}}, k_{\text{des}}) \in K^{(j)}$ such that $k_{\text{init}} = f_{\text{init}}(x_0)$, and construct $\beta_k = \text{diag}(\Delta_K)^{-1} (k - c_K)$. Then

$$\text{slice}\left(Z_{\text{FRS}}^{(i,j,h)}, \beta_k, I\right) \cap O = \emptyset \quad (23)$$

if and only if

$$\text{slice}\left(Z_{\text{slc}}^{(i,j,h)}, \beta_k, \mathbb{N}_{n_K}\right) \not\subset \mathcal{Z}\left(c_{\text{obs}}^{(m)}, [G_{\text{obs}}^{(m)}, G_{\text{extra}}^{(i,j,h)}]\right). \quad (24)$$

Proof. First note, O can be represented as a zonotope because it is a rotated box. Second, notice that, by construction, $Z_{\text{slc}}^{(i,j,h)}$ and $Z_{\text{extra}}^{(i,j,h)} \subset P$. Furthermore, $Z_{\text{slc}}^{(i,j,h)}$ contains the generators of $Z_{\text{FRS}}^{(i,j,h)}$ that can be sliced by β_k [17, Lemma 6.5], and $Z_{\text{extra}}^{(i,j,h)}$ contains all of the other generators (hence the multi-index $\mathbb{N}_n \setminus I$). Finally, it follows from (18) that $\text{slice}\left(Z_{\text{slc}}^{(i,j,h)}, \beta_k, \mathbb{N}_{n_K}\right) \in P$, because $Z_{\text{slc}}^{(i,j,h)}$ has exactly \mathbb{N}_{n_K} generators [17, Lemma 6.5]. The desired result then follows from [20, Lemma 5.1]. \square

Lemma 1 tests if k is unsafe by checking if the sliced FRS zonotope (which is a point) lies inside an obstacle augmented with the “extra” generators of the FRS zonotope.

However, testing if a point is inside a zonotope is not trivial. To address this, note that zonotopes are convex polytopes [20]. So, from [21, Thm. 2.1], we can represent the zonotope $\mathcal{Z}\left(c_{\text{obs}}^{(m)}, [G_{\text{obs}}^{(m)}, G_{\text{extra}}^{(i,j,h)}]\right)$ as the intersection of $n_{\text{hp}} \in \mathbb{N}$ affine halfplanes using a pair of matrices

$$A_{\text{obs}}^{(i,j,h,m)} \in \mathbb{R}^{n_{\text{hp}} \times n_P} \quad \text{and} \quad b_{\text{obs}}^{(i,j,h,m)} \in \mathbb{R}^{n_{\text{hp}} \times 1} \quad (25)$$

for which (24) holds if and only if

$$-\max\left(A_{\text{obs}}^{(i,j,h,m)} \text{slice}(Z_{\text{slc}}, \beta_k, \mathbb{N}_{n_K}) - b_{\text{obs}}^{(i,j,h,m)}\right) < 0, \quad (26)$$

where the max is taken over the elements of its argument. Note $A_{\text{obs}}^{(i,j,h,m)}$ and $b_{\text{obs}}^{(i,j,h,m)}$ can be constructed quickly enough for real-time planning [13], [18].

3) *Parameter Adjustment*: To enforce safety at runtime, we use (26) as a constraint on the RL agent’s choice of k . Using Alg. 1, we adjust an unsafe choice of k by attempting to replace it with a safe one. Importantly, Alg. 1 also returns the Euclidean distance from the RL agent’s choice to the adjusted k , which we use as a penalty during training.

Algorithm 1: $(k, d) = \text{adjust}(x_0, \{O^{(m)}\}_{m=1}^{n_{\text{obs}}}, k_{\text{RL}})$

```

1 get  $Z_{\text{plan}}^{(i,j)}$  and  $Z_{\text{err}}^{(i,j,h)}$  for each  $i \in \mathbb{N}_{m_T}$  using  $x_0$ 
2 create  $Z_{\text{FRS}}^{(i,j,h)}$  for each  $i \in \mathbb{N}_{m_T}$  as in (17)
3 for  $i \in \mathbb{N}_{m_T}, m \in \mathbb{N}_{n_{\text{obs}}}$  do
4   | construct  $A_{\text{obs}}^{(i,j,h,m)}$  and  $b_{\text{obs}}^{(i,j,h,m)}$  as in Sec. IV-A.2
5   | evaluate (26) on  $k_{\text{RL}}$ 
6 end
7 if  $k_{\text{RL}}$  does not satisfy (26) for all  $(i, m)$  then
8   | create a set  $\{k^{(n)}\}_{n=1}^{n_{\text{sample}}}$  of samples in  $K^{(j)}$  such
9   | that  $k_{\text{init}}^{(n)} = f_{\text{init}}(x_0)$  for all  $m$ 
10  | for  $i \in \mathbb{N}_{m_T}, m \in \mathbb{N}_{n_{\text{obs}}}, n \in \mathbb{N}_{n_{\text{sample}}}$  do
11  | | evaluate (26) on each  $k^{(n)}$ 
12  | | end
13  | | if any  $k^{(n)}$  satisfy (26) for all  $(i, m)$  then
14  | | | return  $(k^{(n)}, \|k^{(n)} - k_{\text{RL}}\|_2)$  for which  $k^{(n)}$ 
15  | | | minimizes  $\|k^{(n)} - k_{\text{RL}}\|_2$  and satisfies (26)
16  | | else
17  | | | return  $([], [])$  (robot continues previous plan)
18  | | end
19 end

```

B. Safe Learning with RTS

We use RTS to safely train a model-free RL agent with Alg. 2. Note, our method can be applied to a variety of RL agents such as DDPG and TD3 (see Sec. V). Each training episode in Alg. 2 consists of the robot attempting a task (e.g., reaching a goal position). An episode lasts until the

robot completes the task, crashes, or exceeds a time limit. In each episode, the robot uses RTS+RL to perform receding-horizon planning.

In each planning iteration, we roll out the current policy to get a plan, then adjust the plan if it is unsafe, and finally execute either the new or previous plan. We also train the RL agent on minibatches of *experiences* containing observations, reward, and output of the current policy. The *observations* contain the robot’s state and nearby obstacles (represented, e.g., as an occupancy grid), before and after each planning iteration. The *reward* is a function of the task, robot trajectory, obstacles, and distance that Alg. 1 adjusted the agent’s plan. Note, in practice, training the agent in each planning iteration does not impede the real-time performance of RTS+RL because we use minibatches, and the RL agent can be trained in parallel to the robot executing each plan. We conclude by confirming that RTS+RL is safe:

Theorem 2. *Suppose the ERS satisfies (12). Then an RL agent / robot using Alg. 2 is safe during training.*

Proof. In each planning iteration, Alg. 2 checks if the plan from the RL agent is unsafe using Alg. 1, which either returns a safe plan (by Lem. 1), or else the robot executes a previously-found, safe failsafe maneuver. Since the robot is initialized with a failsafe maneuver, it is always safe. \square

While we do not certify the robot can complete every task, we show next that enforcing safety during training *reduces* how much training an RL agent needs to complete tasks.

V. EXPERIMENTS

The proposed approach is demonstrated on three robotic platforms: a cartpole, a car, and a quadrotor drone. We simulate the robots with realistic high-fidelity models in MATLAB, and use `ode45` to integrate each robot’s dynamics. For each robot, we train two RL agents: one agent with RTS to ensure safety, and a baseline agent with the same planning model (i.e., trajectory parameterization) and tracking controller, but no safety guarantees. We compare the agents’ performance on 500 episodes, with random initial conditions for the cartpole and random obstacles for the car and drone. We present each robot separately; however, due to space limitations, the cartpole is presented in the supplementary material. The supplement also provides implementation details. A supplementary video shows highlights our method’s performance.

A. Car Lane Change Experiment

1) *Task:* This experiment requires an RL agent to plan for a self-driving car to reach a goal position 500 m away on a road-like obstacle course. In this safety-critical application, using baseline RL can lead to collisions. We employ a realistic dynamics model [22] with a larger turning radius at higher speeds, so the car must slow down to avoid obstacles, and stop if there is not enough room to avoid an obstacle.

Algorithm 2: Safe Reinforcement Learning

```

1 initialize random policy and empty experience set  $\mathcal{E}$ 
2 for each training episode do
3   initialize robot at random start position
4   initialize task  $\mathcal{T}$  (e.g., reach a goal position)
5   create random obstacles  $\mathcal{O} = \{O^{(m)}\}_{m=1}^{n_{\text{obs}}}$ 
6   initialize failsafe maneuver (stay at start position)
7   while time limit not exceeded do
8     get initial condition  $x_0$  from robot
9     get observation  $o = \text{observe}(x_0, \mathcal{O})$ 
10    get  $k_{\text{RL}} = \text{rollout}(o)$ 
11    get  $(k_{\text{safe}}, d) = \text{adjust}(x_0, \mathcal{O}, k_{\text{RL}})$  with Alg. 1
12    if  $k_{\text{safe}} \neq []$  then
13      get robot trajectory  $x$  as in (5) by tracking
14       $p_{\text{plan}}(\cdot, k_{\text{safe}})$  for  $t_{\text{plan}}$  s
15      store  $p_{\text{plan}}$  as new failsafe maneuver
16    else
17      get robot trajectory  $x$  as in (5) by
18      continuing previous failsafe for  $t_{\text{plan}}$  s
19    end
20    get  $r = \text{reward}(\mathcal{T}, x, \mathcal{O}, d)$ 
21    get observation  $o' = \text{observe}(x(t_{\text{plan}}), \mathcal{O})$ 
22    store experience  $(o, o', r, k_{\text{RL}})$  in  $\mathcal{E}$ 
23    train policy on a minibatch of  $\mathcal{E}$ 
24    if task  $\mathcal{T}$  done or robot crashed then break
25  end
26 end
27 return trained policy

```

2) *Method and Hypotheses:* We perform training using a TD3 [23] agents for 35,000 episodes. We evaluate the learned policy on 500 additional episodes with randomly placed obstacles. We expect the agent without a safety layer to have many collisions early in training due to choosing speeds that are too high for a safe lane change. After training, we expect both agents to slow the car to avoid obstacles.

3) *Results and Discussion:* Training and evaluation data are shown in Table I. The time per step to run the RTS+RL framework (i.e. the time to run the while loop in Alg. 2) does not incur a large overhead over the baseline approach. Since the time spent ensuring safety and training is an order of magnitude less than $t_{\text{plan}} = 2$ s, our algorithm can be used to ensure RL safety online in real time. Also note that RTS+RL maintains safety during both training and evaluation, in contrast to baseline RL.

The reward during training is shown in Fig. 3. Note, the reward per episode of baseline RL degrades during training because it struggles to balance the reward from traveling at a high speed versus the penalty of avoiding collision. In contrast, RTS+RL rapidly attains high reward, because it does not have to make this same tradeoff. In general, the RTS+RL agent drives more quickly when obstacles are farther away, thereby gaining higher reward per episode. On the other hand, the baseline RL agent travels more slowly to ensure enough time for lane change, but still suffers

Car Lane Change Results	RTS+RL	Baseline RL
<i>Training (35k episodes)</i>		
mean time per step [s]	0.127	0.036
collisions [%]	0.0	72.1
<i>Evaluation (500 episodes)</i>		
collisions [%]	0.0	25.0
reached goal [%]	85.8	75.0
safely stopped [%]	14.2	0.0
safety interventions [%]	4.4	N/A
mean reward per goal reached	538.2	483.6

TABLE I

Performance of RTS+RL vs. baseline RL on the car.



Fig. 3. Reward during training for the car lane change task. The RTS+RL framework (green) is able to more rapidly converge to a high reward policy when compared to a baseline RL approach (red).

collisions. Figure 4 illustrates this: RTS+RL achieves two safe lane changes at high speed, whereas the baseline RL agent has a collision.

Also note, the dynamics we use for RTS+RL have been shown to accurately represent real autonomous car-like robots with a safety layer [12], [24], so we expect that our RTS+RL approach can transfer to real robots.

B. Drone Obstacle Gauntlet Experiment

1) *Task*: We require a quadrotor drone to traverse a 100 m tunnel as quickly as possible while avoiding randomly-placed obstacles. Navigating a drone safely at high speed is challenging in cluttered environments as in Fig. 5. Recent applications of deep/reinforcement learning for drone control and navigation have only empirically demonstrated safety of a learned policy [25]–[27]. We use RL+RTS to enable more systematic guarantees for learning drone navigation.

2) *Method and Hypotheses*: We train RTS+RL and baseline RL using TD3 agents and 3500 episodes, then evaluate both agents on 500 episodes with random obstacles. We expect the RTS+RL agent to have no collisions in training or evaluation, the baseline RL agent to have many collisions during the early part of training, and both agents to eventually navigate each random scenario.

3) *Results and Discussion*: Training and evaluation data are shown in Table II. Note that the RTS+RL time per step is under 0.5 s, less than $t_{\text{plan}} = 0.75$ s required for real-time planning. As expected, RTS+RL had no collisions, whereas the baseline collided in nearly 80% of episodes in training. This is because RTS+RL did not need to explore the penalty associated with crashing, so it learned to maximize reward by completing most of the random scenarios. In contrast,

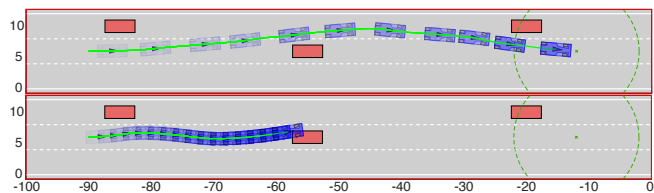


Fig. 4. Car lane changes with RTS+RL (top) and baseline RL (bottom). The car (blue) is plotted at each receding-horizon planning iteration (increasing opacity with time). RTS+RL avoids obstacles (red) while traveling at a higher speed than the baseline RL agent, which suffers a collision.

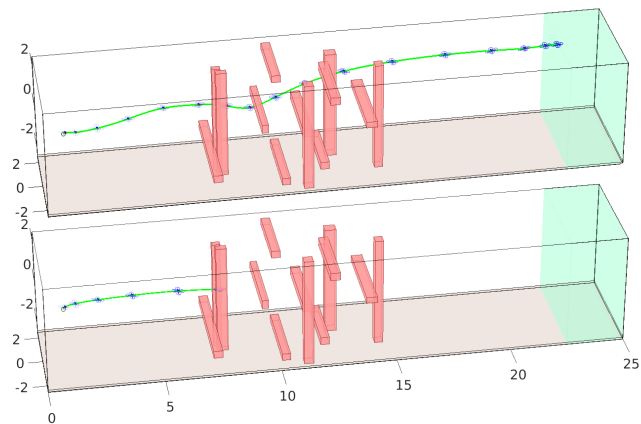


Fig. 5. Drone simulation using RTS+RL (top) vs. baseline RL (bottom). The drone begins on the left and must reach the goal (green) on the right while avoiding obstacles (red). The baseline approach collides with an obstacle in this example. Note, this example world is only 25 m long for illustration purposes. The training/evaluation worlds are 100 m long and more dense.

baseline RL learned to minimize the penalty of collision with obstacles by hovering. This is shown in Fig. 6, where the baseline agent spends the first 2800 episodes learning to avoid collisions near the obstacle-free start location of each scenario, and the remaining learning to fly towards the goal, but then hover instead of flying through the gauntlet; this is also shown in the supplemental video. This problem may be solved by using a larger neural network, longer training, or tuning the reward function; but RTS+RL does not need any of these concessions to succeed.

VI. CONCLUSION

To apply RL on real-world robots in safety-critical environments, one should be able to ensure safety during and after training. To that end, this paper proposes Reachability-based Trajectory Safeguard (RTS), which leverages offline reachability analysis to guarantee safety during training and evaluation. The method, RTS+RL, is demonstrated in simulation performing safe, real-time receding-horizon planning on three robot platforms with continuous action spaces. Importantly, RTS+RL consistently achieves higher rewards in fewer training episodes than a baseline RL method without safety guarantees. Furthermore, the proposed method simplifies RL training by allowing users to focus on designing a reward without having to incorporate penalties for safety. As



Fig. 6. Reward during training for the drone obstacle gauntlet. Our RTS+RL framework (green) learns to navigate the random obstacle gauntlets, whereas the baseline RL approach (red) struggles to accumulate reward, and instead minimizes the penalty of colliding with obstacles by learning to hover in place.

Drone Obstacle Gauntlet Results	RTS+RL	Baseline RL
<i>Training (3500 episodes)</i>		
mean time per step [s]	0.48	0.21
collisions [%]	0.0	79.6
<i>Evaluation (500 episodes)</i>		
collisions [%]	0.0	0.0
reached goal [%]	100.0	0.0
safely stopped [%]	0.0	100.0
safety interventions [%]	39.1	N/A
mean reward per goal reached	196.9	N/A

TABLE II

Performance of RTS+RL vs. baseline RL on the drone.

as a result, the RL agent can learn a safe policy that maximizes a user specified reward. Future work will apply RTS+RL on hardware and non-rigid-body robots, and explore additional benefits of safety guarantees during training.

REFERENCES

- [1] T. Haarnoja, A. Zhou, P. Abbeel, and S. Levine, "Soft actor-critic: Off-policy maximum entropy deep reinforcement learning with a stochastic actor," *arXiv preprint arXiv:1801.01290*, 2018.
- [2] S. Fujimoto, H. Van Hoof, and D. Meger, "Addressing function approximation error in actor-critic methods," *arXiv preprint arXiv:1802.09477*, 2018.
- [3] G. Dalal, K. Dvijotham, M. Vecerik, T. Hester, C. Paduraru, and Y. Tassa, "Safe exploration in continuous action spaces," *arXiv preprint arXiv:1801.08757*, 2018.
- [4] J. Schulman, S. Levine, P. Abbeel, M. Jordan, and P. Moritz, "Trust region policy optimization," in *International conference on machine learning*, 2015, pp. 1889–1897.
- [5] J. Achiam, D. Held, A. Tamar, and P. Abbeel, "Constrained policy optimization," *arXiv preprint arXiv:1705.10528*, 2017.
- [6] F. Berkenkamp, M. Turchetta, A. Schoellig, and A. Krause, "Safe model-based reinforcement learning with stability guarantees," in *Advances in neural information processing systems*, 2017, pp. 908–918.
- [7] R. Cheng, G. Orosz, R. M. Murray, and J. W. Burdick, "End-to-end safe reinforcement learning through barrier functions for safety-critical continuous control tasks," in *Proceedings of the AAAI Conference on Artificial Intelligence*, vol. 33, 2019, pp. 3387–3395.
- [8] J. F. Fisac, A. K. Akametalu, M. N. Zeilinger, S. Kaynama, J. Gillula, and C. J. Tomlin, "A general safety framework for learning-based control in uncertain robotic systems," *IEEE Transactions on Automatic Control*, vol. 64, no. 7, pp. 2737–2752, 2018.
- [9] T. Lew, A. Sharma, J. Harrison, and M. Pavone, "Safe Model-Based Meta-Reinforcement Learning: A Sequential Exploration-Exploitation Framework," *arXiv preprint arXiv:2008.11700*, 2020.
- [10] S. Shalev-Shwartz, S. Shammah, and A. Shashua, "Safe, multi-agent, reinforcement learning for autonomous driving," *arXiv preprint arXiv:1610.03295*, 2016.
- [11] H. Krasowski, X. Wang, and M. Althoff, "Safe reinforcement learning for autonomous lane changing using set-based prediction," in *IEEE International Conference on Intelligent Transportation Systems (ITSC)*, 2020.
- [12] S. Kousik*, S. Vaskov*, F. Bu, M. Johnson-Roberson, and R. Vasudevan, "Bridging the gap between safety and real-time performance in receding-horizon trajectory design for mobile robots," *The International Journal of Robotics Research*, 2020.
- [13] P. Holmes, S. Kousik, B. Zhang, D. Raz, C. Barbalata, M. Johnson-Roberson, and R. Vasudevan, "Reachable Sets for Safe, Real-Time Manipulator Trajectory Design," *Robotics: Science and Systems*, 2019.
- [14] A. Bochkovskiy, C.-Y. Wang, and H.-Y. M. Liao, "Yolov4: Optimal speed and accuracy of object detection," *arXiv preprint arXiv:2004.10934*, 2020.
- [15] S. Thrun, "Robotic mapping: A survey," 2003.
- [16] M. Althoff, "An introduction to cora 2015," in *Proc. of the Workshop on Applied Verification for Continuous and Hybrid Systems*, 2015.
- [17] S. Kousik, "Reachability-based Trajectory Design," Ph.D. dissertation, University of Michigan, 2020.
- [18] S. Kousik, P. Holmes, and R. Vasudevan, "Safe, aggressive quadrotor flight via reachability-based trajectory design," in *Dynamic Systems and Control Conference*, American Society of Mechanical Engineers, vol. 59162, 2019, V003T19A010.
- [19] C.-T. Chang, B. Gorissen, and S. Melchior, "Fast Oriented Bounding Box Optimization on the Rotation Group SO(3)," *ACM Trans. Graph.*, vol. 30, no. 5, Oct. 2011.
- [20] L. J. Guibas, A. T. Nguyen, and L. Zhang, "Zonotopes as bounding volumes," in *SODA*, vol. 3, 2003, pp. 803–812.
- [21] M. Althoff, "Reachability analysis and its application to the safety assessment of autonomous cars," Ph.D. dissertation, Technische Universität München, 2010.
- [22] Y. Rasekhipour, A. Khajepour, S.-K. Chen, and B. Litkouhi, "A potential field-based model predictive path-planning controller for autonomous road vehicles," *IEEE Transactions on Intelligent Transportation Systems*, vol. 18, no. 5, pp. 1255–1267, 2016.
- [23] S. Fujimoto, H. Van Hoof, and D. Meger, "Addressing function approximation error in actor-critic methods," *arXiv preprint arXiv:1802.09477*, 2018.
- [24] S. Vaskov, S. Kousik, H. Larson, F. Bu, J. Ward, S. Worrall, M. Johnson-Roberson, and R. Vasudevan, "Towards provably not-at-fault control of autonomous robots in arbitrary dynamic environments," *arXiv preprint arXiv:1902.02851*, 2019.
- [25] J. Hwangbo, I. Sa, R. Siegwart, and M. Hutter, "Control of a quadrotor with reinforcement learning," *IEEE Robotics and Automation Letters*, vol. 2, no. 4, pp. 2096–2103, 2017.
- [26] S. L. Waslander, G. M. Hoffmann, J. S. Jang, and C. J. Tomlin, "Multi-agent quadrotor testbed control design: Integral sliding mode vs. reinforcement learning," in *2005 IEEE/RSJ International Conference on Intelligent Robots and Systems*, IEEE, 2005, pp. 3712–3717.
- [27] E. Kaufmann, A. Loquercio, R. Ranftl, M. Müller, V. Koltun, and D. Scaramuzza, "Deep drone acrobatics," *arXiv preprint arXiv:2006.05768*, 2020.
- [28] S. Kousik, B. Zhang, P. Zhao, and R. Vasudevan, "Safe, Optimal, Real-time Trajectory Planning with a Parallel Constrained Bernstein Algorithm," *IEEE Transactions on Robotics*, 2020, in press.
- [29] S. Vaskov, H. Larson, S. Kousik, M. Johnson-Roberson, and R. Vasudevan, "Not-at-fault driving in traffic: A reachability-based approach," in *2019 IEEE Intelligent Transportation Systems Conference (ITSC)*, IEEE, 2019, pp. 2785–2790.
- [30] J. R. Pati, "Modeling, identification and control of cart-pole system," 2014.
- [31] T. P. Lillicrap, J. J. Hunt, A. Pritzel, N. Heess, T. Erez, Y. Tassa, D. Silver, and D. Wierstra, "Continuous control with deep reinforcement learning," *arXiv preprint arXiv:1509.02971*, 2015.
- [32] M. W. Mueller, M. Hehn, and R. D'Andrea, "A computationally efficient motion primitive for quadcopter trajectory generation," *IEEE Transactions on Robotics*, vol. 31, no. 6, pp. 1294–1310, 2015.
- [33] T. Lee, M. Leok, and N. H. McClamroch, "Geometric tracking control of a quadrotor uav on se(3)," in *49th IEEE Conference on Decision and Control (CDC)*, 2010, pp. 5420–5425.

In this supplement, we provide the following. First, we justify why our sampling-based reachability analysis to compute the ERS results in a conservative representation. Second, we inspect the structure of the FRS to clarify the utility of the slicing operation. Third, we present the cartpole experiment results. Fourth, fifth, and sixth, we provide implementation details for the cartpole, car, and drone robots. In particular, we present the high-fidelity model, planning model, tracking controller, and RL reward function for each robot.

A. Justifying ERS Conservatism

We now justify why we sample the *corners* of each $K^{(j)} \times X_0^{(h)}$ to ensure that our ERS representation is conservative as in (12). In short, as one would expect, tracking error is maximized by sampling the largest possible commanded *changes* in the robot's velocity. When a planning model's velocity is monotonic in k_{init} and/or k_{des} (which the models we consider are), this implies that one should choose samples of k with the largest possible magnitude.

As a reminder, we require conservatism because, if we *overestimate* the robot's reachable set, then we can ensure the robot is safe by ensuring that its reachable set does not intersect obstacles.

Note that it is reasonable to satisfy (12) in practice, as validated empirically in both simulation and on hardware for a variety of robot morphologies [12], [13], [17], [18], [24], [28], [29]. Moreover, if one is unsure if (12) is satisfied, one can simply use larger $Z_{\text{err}}^{(i,j,h)}$.

We proceed by considering a 1-D linear system representing the robot's actuators. We assume that the robot's tracking error is proportional to its actuators' tracking error with respect to a desired acceleration profile. We also assume that all states in X that are not linear/angular position are the robot's linear/angular velocity; in other words, maximizing acceleration error leads to maximizing position error.

We sample the corners of $X_0^{(h)}$ because tracking error is maximized when initial speed is maximized:

Proposition 3. ([17, Proposition 7.1]) *Consider a 1-D high-fidelity model with states p and $\dot{p} \in \mathbb{R}$, and $\ddot{p} = u \in \mathbb{R}$. Let $p_{\text{plan}}(\cdot, k) : T \rightarrow \mathbb{R}$ be a smooth plan. Suppose that*

$$u = \gamma_p \cdot (p - p_{\text{plan}}) + \gamma_d \cdot (\dot{p} - \dot{p}_{\text{plan}}) + \ddot{p}_{\text{plan}}, \quad (27)$$

where $\gamma_p, \gamma_d \in \mathbb{R}$ are control gains and \ddot{p}_{plan} is a feedforward term. Suppose that $p(0, k) = p_{\text{plan}}(0, k) = 0$ and $\dot{p}(0, k) \in [\dot{p}_{\text{min}}, \dot{p}_{\text{max}}]$. Then the tracking error magnitude $|p(t, k) - p_{\text{plan}}(t, k)|$ achieves a maximum over $t \in T$ and over all $\dot{p}(0, k)$ when $\dot{p}(0, k) \in \{\dot{p}_{\text{min}}, \dot{p}_{\text{max}}\}$.

Recall that we require $k_{\text{init}} = f_{\text{init}}(x_0)$, so this proposition justifies sampling the corners of both $K_{\text{init}}^{(j)}$ and $X_0^{(h)}$.

We sample the corners of $K_{\text{des}}^{(j)}$ because tracking error is maximized when commanded velocity is maximized:

Proposition 4. *Consider the model from Proposition 3, and suppose u has no feedforward term:*

$$u = \gamma_p \cdot (p - p_{\text{plan}}) + \gamma_d \cdot (\dot{p} - \dot{p}_{\text{plan}}). \quad (28)$$

Suppose $p(0) = p_{\text{plan}}(0, k)$. Suppose $k = (k_{\text{init}}, k_{\text{des}})$ with k_{init} fixed such that $\dot{p}(0, k) = \dot{p}_{\text{plan}}(0, k)$. Consider a planning model $p_{\text{plan}} : T \times K \rightarrow \mathbb{R}$ for which, for all $t \in T$, $\ddot{p}_{\text{plan}}(t, k) = k_{\text{des}} \in [k_{\text{min}}, k_{\text{max}}] \subset \mathbb{R}$ (that is, K_{des} is also 1-D). Then the tracking error magnitude $|p(t) - p_{\text{plan}}(t)|$ is maximized when $k_{\text{des}} \in \{k_{\text{min}}, k_{\text{max}}\}$.

Proof. Consider the tracking error system

$$z(t, k) = \begin{bmatrix} z_1(t, k) \\ z_2(t, k) \end{bmatrix} = \begin{bmatrix} p(t) - p_{\text{plan}}(t, k) \\ \dot{p}(t) - \dot{p}_{\text{plan}}(t, k) \end{bmatrix}. \quad (29)$$

Recalling that $\dot{k} = 0$ for any plan, we have

$$\dot{z}(t, k) = \underbrace{\begin{bmatrix} 0 & 1 \\ \gamma_p & \gamma_d \end{bmatrix}}_A z(t, k) + \begin{bmatrix} 0 \\ \ddot{p}_{\text{plan}}(t, k) \end{bmatrix}, \quad (30)$$

for any fixed $k \in K$. We can solve for z to find

$$z(t, k) = e^{At} z(0, k) + \int_0^t e^{A(t-s)} \begin{bmatrix} 0 \\ \ddot{p}_{\text{plan}}(s, k) \end{bmatrix} ds \quad (31)$$

$$= 0 + \left(\int_0^t e^{A(t-s)} ds \right) \begin{bmatrix} 0 \\ k_{\text{des}} \end{bmatrix} \quad (32)$$

$$= -A^{-1} (e^{At} - I_{2 \times 2}) \begin{bmatrix} 0 \\ k_{\text{des}} \end{bmatrix}, \quad (33)$$

where $I_{2 \times 2}$ is an identity matrix. Notice that

$$A^{-1} = \begin{bmatrix} -\gamma_d/\gamma_p & 1/\gamma_p \\ 1 & 0 \end{bmatrix}, \quad (34)$$

and we can choose γ_p and γ_d such that

$$e^{At} = \begin{bmatrix} a_1(t) & a_2(t) \\ a_3(t) & a_4(t) \end{bmatrix} \quad (35)$$

with $a_2(t)$ and $a_4(t) \neq 0$. Then, by expanding (33), we have

$$z_1(t, k) = \frac{1 - \gamma_d a_2(t) + a_4(t)}{\gamma_p} k_{\text{des}}, \quad (36)$$

completing the proof. \square

Note that the planning model in this proposition does not obey the requirement that $\dot{p}_{\text{plan}}(t_{\text{fin}}, k) = 0$. We chose this simplification for the sake of illustrating the main idea: the tracking error is proportional to k_{des} , as one would expect.

Note, one can derive a similar result for a planning model with $\ddot{p}_{\text{plan}}(t, k) \propto (k_{\text{des}} - k_{\text{init}})t^2$ (as is the case for the three robots we consider in this paper) by applying integration by parts to (31). More generally, this result holds (again by applying integration by parts) if $\ddot{p}_{\text{plan}}(t, k) = f_1(k)f_2(t)$ where f_1 is a linear combination of elements of k and f_2 is a polynomial in t .

Furthermore, input saturation does not affect the result of Proposition 4. Notice that we assume the control input is drawn from $U = \mathbb{R}$, but U is compact for the high-fidelity model. First, notice that if we include the feedforward term \ddot{p}_{plan} in u from (28), then the tracking error is 0 for all time without input saturation. But, if the input is saturated, this is equivalent to a constant control input being applied in the solution to (30), meaning that \ddot{p} is a constant as in the proof. Therefore, as we would expect, one can maximize

tracking error by choosing k_{des} to maximize input saturation (i.e., command the largest possible acceleration).

The takeaway is: it is reasonable to assume that, if we compute the ERS zonotopes as in Sec. III-B.3, then they enclose the worst-case tracking error as in (12).

B. Slicing the FRS Zonotopes

To demonstrate the utility of slicing, we check that the FRS does indeed contain the motion of the robot when tracking any plan:

Lemma 5. ([17, Thm. 6.6]) *Suppose $t \in T^{(i)}$. Let $k \in K^{(j)}$. Suppose $Z_{\text{err}}^{(i,j,h)}$ satisfies (12). Let*

$$\beta_k = \text{diag}(\Delta_K)^{-1} (k - c_K). \quad (37)$$

Let $I = \mathbb{N}_{n_K} + n_P$. Then

$$\text{FO}(x(t; x_0, k)) \subset \text{slice}(Z_{\text{FRS}}^{(i,j,h)}, \beta_k, \mathbb{N}_{n_K}). \quad (38)$$

Note, I is constructed in this way because the first n_P columns of the generator matrix correspond to the p_{plan} dimensions of $Z_{\text{FRS}}^{(i,j,h)}$; the next n_K columns correspond to k [17, Lemma 6.5], and all other columns correspond to the ERS zonotope by construction. So, we slice all the generators that correspond to k ; the remaining generators add volume to $Z_{\text{FRS}}^{(i,j,h)}$ to compensate for tracking error, the body of the robot, and nonlinearities in $\dot{p}_{\text{plan}}(\cdot, k)$.

In short, one can slice the FRS to find the reachable volume in workspace corresponding to a particular plan. The plan is safe if this volume does not intersect with obstacles.

C. Cartpole Implementation Details

To demonstrate safe RL on a simple example, we use a cartpole, or an unactuated pendulum on a cart. We consider the swingup task, wherein one must invert the pendulum by moving the cart. We limit the length of track available for the cart to move on, and seek to complete the task using only motion plans that do not overrun the track boundaries. While we do not consider the pendulum for obstacle avoidance (to keep the example simple), this method can extend to including the pendulum using techniques from [13].

1) *High-Fidelity Model:* The cartpole's state is $x = (p, \dot{p}, \theta, \dot{\theta})$, containing the cart position and velocity (p and \dot{p}) and the pendulum angle (relative to vertical) and velocity (θ and $\dot{\theta}$). We use the following high-fidelity model [30]:

$$\ddot{p} = \frac{(w + ml^2)(u + ml\dot{\theta}^2 \sin \theta) - gm^2 l^2 \sin \theta \cos \theta}{w(m_c + m) + ml^2(m_c + m \sin^2 \theta)} \quad (39)$$

$$\ddot{\theta} = \frac{-ml(u \cos \theta + ml\dot{\theta}^2 \sin \theta \cdot \cos \theta - (m_c + m)g \sin \theta)}{w(m_c + m) + ml^2(m_c + m \sin^2 \theta)}, \quad (40)$$

where $w = 0.099 \text{ kg}\cdot\text{m}^2$ is the inertia of the pendulum, $m = 0.2 \text{ kg}$ is the mass of pole, $m_c = 2 \text{ kg}$ is the mass of the cart, and $l = 0.5 \text{ m}$ is the length of the pole [30, Table I, pg. 8]. The control input is u .

For X , we require $p(t) \in [-4, 4] \text{ m}$ (instead of randomizing the track length, we randomize the cart and pendulum initial

state in each episode). We require $\dot{p}(t) \in [-5, 5] \text{ m/s}$, $\theta \in [-\pi, \pi] \text{ rad}$. We do not explicitly bound $\dot{\theta}$. We draw control inputs from $U = [-40, 40] \text{ N}$.

2) *Planning Model:* We use the following planning model for the cartpole, based on the 1-D model in [18]. The trajectory parameters are $(k_v, k_a) \in K_{\text{init}} \subset \mathbb{R}^2$ and $k_{\text{des}} \in K_{\text{des}} \subset \mathbb{R}$; k_v (resp. k_a) is the cart's initial velocity (resp. initial acceleration), and k_{des} is a desired velocity to be achieved at a time $t_{\text{des}} \in (0, t_{\text{fin}})$. The planning model is:

$$p_{\text{plan}}(t, k) = \frac{\tau_1(t, k)}{24} t^4 + \frac{\tau_2(t, k)}{6} t^3 + \frac{k_a}{2} t^2 + k_v t \quad (41)$$

$$\begin{bmatrix} \tau_1(t, k) \\ \tau_2(t, k) \end{bmatrix} = \frac{1}{(\tau_3(t))^3} \begin{bmatrix} -12 & 6\tau_3(t) \\ 6\tau_3(t) & -2(\tau_3(t))^2 \end{bmatrix} \begin{bmatrix} \Delta_v(t, k) \\ \Delta_a(t, k) \end{bmatrix} \quad (42)$$

$$\tau_3(t) = \begin{cases} t_{\text{des}} & t \in [0, t_{\text{des}}) \\ t_{\text{fin}} - t_{\text{des}} & t \in [t_{\text{des}}, t_{\text{fin}}] \end{cases} \quad (43)$$

$$\Delta_v(t, k) = \begin{cases} k_{\text{des}} - k_v - k_a t_{\text{des}} & t \in [0, t_{\text{des}}) \\ -k_{\text{des}} & t \in [t_{\text{des}}, t_{\text{fin}}] \end{cases} \quad (44)$$

$$\Delta_a(t, k) = \begin{cases} -k_a & t \in [0, t_{\text{des}}) \\ 0 & t \in [t_{\text{des}}, t_{\text{fin}}] \end{cases} \quad (45)$$

We set $k_v, k_{\text{des}} \in [-5, 5] \text{ m/s}$ and $k_a \in [-15, 15] \text{ m/s}^2$. We set $t_{\text{plan}} = t_{\text{des}} = 0.1 \text{ s}$ and $t_{\text{fin}} = 0.3 \text{ s}$.

3) *Tracking Controller:* We use

$$u_{\text{trk}}(t, x(t), k) = [\gamma_p, \gamma_d] \cdot \begin{bmatrix} p_{\text{plan}}(t, k) - p(t) \\ \dot{p}_{\text{plan}}(t, k) - \dot{p}(t) \end{bmatrix}, \quad (46)$$

where $\gamma_d = \gamma_p = 50$ are control gains with the appropriate units. We saturate this controller if $|u_{\text{trk}}(\cdot)| > 40 \text{ N}$.

4) *Reachability Hyperparameters:* To compute the PRS and ERS, we partition T into $m_T = 30$ intervals. We partition the k_v dimension of K into 11 intervals and k_a into 5 intervals, so $m_K = 11 \times 5$. We similarly partition the \dot{p} dimension of X_0 into 11 intervals; we partition the θ dimension into 4 intervals, and do not partition the $\dot{\theta}$ dimension, so $m_0 = 11 \times 4$. We found that, since the pendulum is light compared to the cart, the cart's tracking error is not significantly influenced by the pendulum's speed. Also note, we do not need to partition the p dimension of X_0 because all plans start at $p(0) = 0$.

5) *Reward:* We specify three terms for the cartpole reward: r_1 rewards bringing the pendulum upright, r_{sign} rewards the cart being in the middle of the track (by penalizing the cart position and speed having opposite signs), and r_p penalizes the cart overrunning the track boundaries. Recall that $x = (p, \dot{p}, \theta, \dot{\theta}) \in X$.

$$r(x) = r_1(x) + r_2(x) + r_3(x), \text{ where} \quad (47)$$

$$r_1(x) = \frac{1}{2} \cos \theta + \frac{1}{2} \quad (48)$$

$$r_2(x) = -0.1 \cdot \text{sign}(p) \cdot \text{sign}(\dot{p}), \text{ and} \quad (49)$$

$$r_3(x) = \begin{cases} -0.05|p| + 30 & p \in [-4, 4] \\ -0.05|p| - 30 & p \notin [-4, 4]. \end{cases} \quad (50)$$

Here, sign returns $+1$ or -1 (i.e., the sign of its argument).

6) *Observations:* We provide the RL agent with observations of the robot's state: $o = (p, \dot{p}, \sin \theta, \cos \theta, \dot{\theta})$.

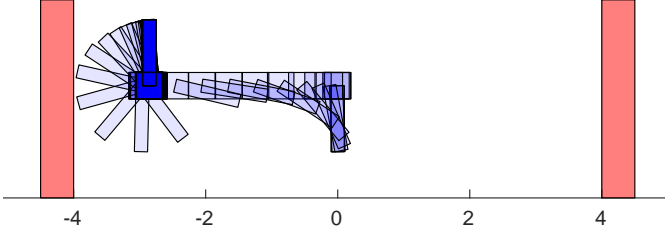


Fig. 7. A time lapse illustration of the cartpole swingup policy learned by our proposed RTS+RL method. The cart is the blue rectangle that moves horizontally, and the pendulum is the blue rectangle that rotates; the red walls are the track boundaries; the track is not shown to reduce visual clutter. The cart begins at 0 and moves to the left, then brakes to a stop before hitting the boundary while still completing the swingup motion. This figure shows a hand-crafted initial condition to emphasize our approach’s ability to obey the constraints; the training and evaluation episodes had randomized initial conditions, but RTS+RL still obeyed the constraints.

D. Cartpole Swing Up Experiment

1) *Task*: As mentioned above, the cartpole task is to swing up the freely-rotating, unactuated pendulum by planning trajectories for the cart while ensuring safety by staying within the track bounds.

2) *Method and Hypotheses*: We train two DDPG [31] RL agents (one with RTS and one without, as noted in Sec. V). Each agent trains for 300 episodes, and then is tested for 500 episodes. Every episode starts with the robot at a random initial cart position, velocity, pendulum angle, and pendulum velocity. We ensure the random position is far enough from the track limits that it is possible to avoid collision.

Since RL optimizes for the long-term reward, we expect both agents to attempt to complete the swingup task. However, we expect RTS will enable the learned policy to *always* respect the track limits. In addition, we expect RTS+RL to learn a successful policy more quickly, since it does not need to explore the penalty incurred by leaving the track boundaries.

3) *Results and Discussion*: We summarize the results in Table III. The reward during training for each RL agent is shown in Fig. 8. As we saw with the car and drone, the RTS+RL agent is able to achieve a higher reward in fewer episodes.

Importantly, the time per step to run the RTS+RL framework (i.e. the time to run the while loop in Algorithm 2) does not create too large an overhead when compared to a baseline approach. In particular, the time per step (which includes ensuring safety) is less than $t_{\text{plan}} = 0.1$ s, so our method can be used to ensure RL safety online.

Both agents are eventually able learn a policy to complete the swing up task, and both obtain similar reward on successful trials. However, only RTS+RL is able to guarantee safety while completing the task. Figure 8 shows that RTS+RL also achieves higher reward for a larger portion of episodes than the baseline.

Cartpole Swing Up Results	RTS+RL	Baseline RL
<i>Training (300 episodes)</i>		
mean time per step [s]	0.041	0.001
collisions [%]	0.0	50.3
<i>Evaluation (500 episodes)</i>		
collisions [%]	0.0	1.0
reached goal [%]	100.0	94.0
safely stopped [%]	0.0	0.0
safety interventions [%]	5.3	N/A
mean reward per goal reached	60.6	61.9

TABLE III

Performance of RTS+RL vs. baseline RL on the cartpole swing up task.

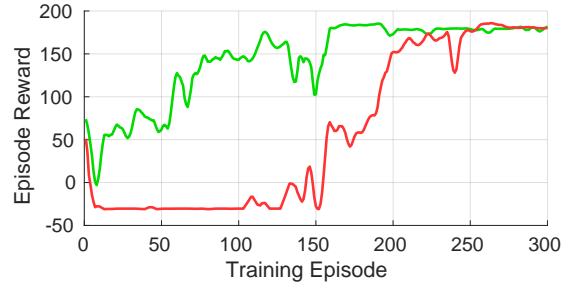


Fig. 8. The training plot for the cartpole swingup task. The RTS+RL framework (green) is able to more rapidly converge to a high reward policy when compared to a baseline RL approach (red).

E. Car Implementation Details

1) *High-Fidelity Model*: We use the following high-fidelity model, adapted from [22] to represent a car driving on a multi-lane road. The state space of the vehicle is $x = [p_{\text{long}}, p_{\text{lat}}, \psi, v, \delta] \in X$, with dynamics

$$\dot{x} = \frac{d}{dt} \begin{bmatrix} p_{\text{long}} \\ p_{\text{lat}} \\ \psi \\ v \\ \delta \end{bmatrix} = \begin{bmatrix} v \cos \psi - v_{\text{lat}} \cos \psi \\ v \sin \psi + v_{\text{lat}} \cos \psi \\ \omega \\ c_1 v + c_2 u_1 \\ c_3 \cdot (u_2 - \delta) \end{bmatrix}, \quad (51)$$

$$\omega = \frac{v \tan \delta}{c_4 + c_5 v^2}, \quad \text{and} \quad (52)$$

$$v_{\text{lat}} = \omega (c_6 + c_7 v^2), \quad (53)$$

where p_{long} , p_{lat} , and ψ are the longitudinal, lateral position, and heading in the global reference frame; v is the longitudinal velocity in the robot’s local (body-fixed) coordinate frame (v_{lat} is its lateral velocity), and δ is its steering angle. The control inputs are $u = [u_1, u_2]^T \in U$ are the acceleration command u_1 and steering torque u_2 . The values $c_1, \dots, c_7 \in \mathbb{R}$ are constant model parameters.

We specify $\psi \in [-0.3, +0.3]$ rad, $v \in [0, 5]$ m/s, $\delta \in [-0.1, 0.1]$ rad. The control inputs are drawn from $u_1 \in [-4, 4]$ m/s² and $u_2 \in [-2, 2]$ rad/s.

2) *Planning Model*: We specify the car’s planning model using piecewise polynomials adapted from [32]. Recall that $p = (p_{\text{long}}, p_{\text{lat}})$ for this model. Let $K_{\text{init}}, K_{\text{des}} \subset \mathbb{R}^2$, and denote $k = (k_{\text{init}}^{[1]}, k_{\text{init}}^{[2]}, k_{\text{des}}^{[1]}, k_{\text{des}}^{[2]}) \in K$. The parameter $k_{\text{des}}^{[1]}$ specifies a velocity to be reached at a time $t_{\text{des}}^{[1]} \in (0, t_{\text{fin}})$, and $k_{\text{des}}^{[2]}$ specifies a lateral position to be reached at a time

$t_{\text{des}}^{[2]} \in (0, t_{\text{fin}})$. Denote $p_{\text{plan}} = (p_1, p_2)$. The planning model is

$$p_1(t, k) = \frac{\tau_1(t, k)}{24} t^4 + \frac{\tau_2(t, k)}{6} t^3 + k_{\text{init}}^{[1]} t, \quad (54)$$

$$p_2(t, k) = \frac{\tau_4(t, k)}{120} t^5 + \frac{\tau_5(t, k)}{24} t^4 + \frac{\tau_6(t, k)}{6} t^3 - \Delta_{v_{\text{lat}}}(k) t, \quad (55)$$

where τ_1, \dots, τ_7 are given by

$$\begin{bmatrix} \tau_1(t, k) \\ \tau_2(t, k) \end{bmatrix} = \frac{\Delta_{v_{\text{long}}}(t, k)}{(\tau_3(t))^3} \begin{bmatrix} -12 \\ 6\tau_3(t) \end{bmatrix} \text{ and} \quad (56)$$

$$\begin{bmatrix} \tau_4(t, k) \\ \tau_5(t, k) \\ \tau_6(t, k) \end{bmatrix} = \frac{1}{(\tau_7(t))^5} \begin{bmatrix} 720 & -360\tau_7(t) \\ -360\tau_7(t) & 168\tau_7(t)^2 \\ 60\tau_7(t)^2 & -24\tau_7(t)^3 \end{bmatrix} \Delta_{\text{lat}}(t, k), \quad (57)$$

which are piecewise constant in t because

$$\tau_3(t) = \begin{cases} t_{\text{des}}^{[1]} & t \in [0, t_{\text{des}}^{[1]}) \\ t_{\text{fin}} - t_{\text{des}}^{[1]} & t \in [t_{\text{des}}^{[1]}, t_{\text{fin}}] \end{cases}, \quad (58)$$

$$\tau_7(t) = \begin{cases} t_{\text{des}}^{[2]} & t \in [0, t_{\text{des}}^{[2]}) \\ t_{\text{fin}} - t_{\text{des}}^{[2]} & t \in [t_{\text{des}}^{[2]}, t_{\text{fin}}] \end{cases}, \quad (59)$$

and each $\Delta_{(\cdot)}$ is given by

$$\Delta_{\text{lat}}(t, k) = \begin{bmatrix} \Delta_{p_{\text{lat}}}(t, k) \\ \Delta_{v_{\text{lat}}}(t, k) \end{bmatrix}, \quad (60)$$

$$\Delta_{v_{\text{long}}}(t, k) = \begin{cases} k_{\text{des}}^{[1]} - k_{\text{init}}^{[1]} & t \in [0, t_{\text{des}}^{[1]}) \\ -k_{\text{des}}^{[1]} & t \in [t_{\text{des}}^{[1]}, t_{\text{fin}}] \end{cases}, \quad (61)$$

$$\Delta_{p_{\text{lat}}}(t, k) = \begin{cases} k_{\text{des}}^{[2]} - \Delta_{v_{\text{lat}}}(t, k) & t \in [0, t_{\text{des}}^{[2]}) \\ 0 & t \in [t_{\text{des}}^{[2]}, t_{\text{fin}}] \end{cases}, \text{ and} \quad (62)$$

$$\Delta_{v_{\text{lat}}}(t, k) = \begin{cases} -k_{\text{init}}^{[1]} \sin(k_{\text{init}}^{[2]}) & t \in [0, t_{\text{des}}^{[2]}) \\ 0 & t \in [t_{\text{des}}^{[2]}, t_{\text{fin}}] \end{cases}. \quad (63)$$

Example plans are shown in Figure 9.

We specify $k_{\text{init}}^{[1]}, k_{\text{des}}^{[1]} \in [0, 5]$ m/s and $k_{\text{init}}^{[2]}, k_{\text{des}}^{[2]} \in [-1, 1]$ m. We set the timing parameters as $t_{\text{plan}} = 2$ s, $t_{\text{des}}^{[1]} = 2$ s, $t_{\text{des}}^{[2]} = 4$ s, and $t_{\text{fin}} = 6$ s. Note, as we see in the results in Sec. V of the paper, the car consistently finds new plans in ≈ 0.1 s. However, we chose $t_{\text{plan}} = 2$ s because we found that this reduced oscillations due to the RL agents choosing frequent lane changes, which improved the agents' ability to complete the car lane change task.

3) *Tracking Controller*: Recall that $P = P_{\text{long}} \times P_{\text{lat}}$ and $x = (p, \psi, v, \delta) \in \mathbb{R}^5$. Let p_{plan} be a plan with k_{init} determined by x . We specify u_{trk} for the car as a PD controller:

$$u_{\text{trk}}(t, x(t)) = \Gamma \cdot \left(\begin{bmatrix} p(t) \\ \psi(t) \\ v(t) \\ \delta(t) \end{bmatrix} - \begin{bmatrix} p_{\text{plan}}(t, k) + p_0 \\ 0 \\ \dot{p}_1(t, k) \\ 0 \end{bmatrix} \right), \quad (64)$$

where $\Gamma \in \mathbb{R}^{2 \times 5}$ is a matrix of control gains, $p_0 = \text{proj}_P(x(0))$, and \dot{p}_1 is the time derivative of (54).

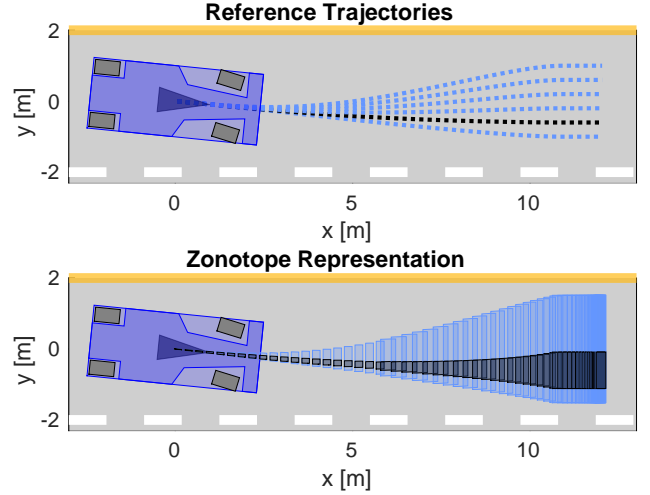


Fig. 9. The top subfigure shows plans for the car at different $k_{\text{des}}^{[2]}$ parameter values ranging from $[-1, 1]$ m, with one specific trajectory shown in black. The bottom subfigure shows the zonotope PRS for the same range of $k_{\text{des}}^{[2]}$. The black subset is the sliced PRS corresponding to the trajectory in the top subfigure. Notice that it conservatively contains the given trajectory.

4) *Reachability Hyperparameters*: To compute the PRS and ERS, we partition T into $m_T = 120$ intervals of duration $\Delta_T = 0.05$ s. We partition $k_{\text{init}}^{[1]}$ into 2 intervals, and do not partition $k_{\text{init}}^{[2]}$, so $m_K = 2$. We partition the θ dimension of X_0 into 13 intervals, the v dimension into 2 intervals, and the δ dimension into 5 intervals, so $m_0 = 13 \times 2 \times 5$.

5) *Reward*: Recall the robot's state is $x = (p_{\text{long}}, p_{\text{lat}}, \psi, v, \delta)$. The total reward consists of a speed reward, a lane reward and goal reward:

$$r(x) = r_{\text{speed}}(x) + r_{\text{lane}}(x) + r_{\text{goal}}(x) \quad (65)$$

The speed reward is

$$r_{\text{speed}} = \exp\left(\frac{-1}{v^2 + 1}\right) - 2. \quad (66)$$

The lane reward encourages the car to stay in one of three lanes in the road-like environment:

$$r_{\text{lane}} = \begin{cases} 5 \exp\left(\frac{-1}{(y_{\text{obs}} - 2)^2 + 1}\right) - 2 |p_{\text{lat}} - 2| & p_{\text{lat}} \in [0, 2) \\ 5 \exp\left(\frac{-1}{p_{\text{lat}}^2 + 1}\right) & p_{\text{lat}} \in [2, 10) \\ 5 \exp\left(\frac{-1}{(y_{\text{obs}} - 10)^2 + 1}\right) - 2 |p_{\text{lat}} - 10| & p_{\text{lat}} \in [10, 12] \end{cases}. \quad (67)$$

Finally, the goal reward encourages maintaining a high average velocity and reaching the end of the road

$$r_{\text{goal}} = \begin{cases} 0 & p_{\text{long}} < 500 \\ 10v_{\text{avg}} + 30 & p_{\text{long}} \geq 500 \end{cases} \quad (68)$$

where v_{avg} is the average of the car's velocity state v over the entire episode. Notice we require the car to drive for 500 m in each episode.

6) *Observations*: We specify five elements for the car’s observations. The first two are the distance in global coordinates from the car’s center of mass to the closest obstacle in front of the car, Δ_{long} and Δ_{lat} . The last three observations are the car’s global position and velocity, p_{long} , p_{lat} , and v . So,

$$o = (\Delta_{\text{long}}, \Delta_{\text{lat}}, p_{\text{long}}, p_{\text{lat}}, v). \quad (69)$$

F. Drone Implementation Details

1) *High-fidelity Model*: We use the following high-fidelity model for the drone [33]:

$$\ddot{p} = \tau Re_3 - mge_3 \quad (70)$$

$$\dot{R} = R\hat{\omega} \quad (71)$$

$$\dot{\omega} = J^{-1}(\mu - \omega \times J\omega), \quad (72)$$

with states for position $p \in \mathbb{R}^3$, velocity $\dot{p} \in \mathbb{R}^3$, attitude $R \in \text{SO}(3)$, and angular velocity $\omega \in \mathbb{R}^3$. The model has been modified from [33] to use a north-west-up convention for the global and body frame coordinate axes; e_3 is the global up direction.

Its control inputs $u = (\tau, \mu) \in U \subset \mathbb{R}^4$ are thrust $\tau > 0$ and body moment $\mu \in \mathbb{R}^3$. We convert these control inputs (given by a tracking controller described below) to rotor speeds using [18, (3)], then saturate the rotor speeds to enforce compactness of U .

We use model parameters for an AscTec Hummingbird drone with mass $m = 0.547$ kg and moment of inertia tensor $J = 10^{-3} \cdot \text{diag}(3.3, 3.3, 5.8)$ kgm/s². We set $g = 9.81$ m/s². The rotor speeds (and therefore the control inputs) are saturated to within [1100, 8600] rpm. See [18, Table I] for more details. This model does not include aerodynamic drag, so it is valid up to a maximum speed of $\|\dot{p}(t)\|_2 = 5$ m/s [18]. Further bounds on the states and inputs are in [18].

2) *Planning Model*: The drone uses the same planning model as the cartpole separately in each of the three directions of \mathbb{R}^3 . We bound its velocity parameter to $[-5, 5]$ m/s, and its initial acceleration to $[-10, 10]$ m/s². We pick $t_{\text{plan}} = 0.5$ s, $t_{\text{des}} = 1.5$ s, and $t_{\text{fin}} = 3$ s. See [18] and [17] for more details about the planning model, PRS computation, and ERS computation.

3) *Tracking Controller*: We use the tracking controller developed in [33], which has stronger stability guarantees than the controller used in [18], which we found in practice enables the RL agent to choose more aggressive trajectories while maintaining safety. Per the notation in [33], we set the control gains as $k_x = 2$, $k_v = 0.5$, $k_R = 1$, and $k_\Omega = 0.03$.

4) *Reward*: We construct the reward as

$$r(x) = r_v(x) + r_{\text{obs}}(x). \quad (73)$$

The first term rewards traveling in the direction of the goal:

$$r_v = \frac{1}{2} e_{\text{goal}} \cdot \dot{p}, \quad (74)$$

where e_{goal} is a unit vector from the drone’s global position p to the global goal location, and \dot{p} is the drone’s velocity

(so \cdot indicates the dot product). The second term penalizes being near obstacles:

$$r_{\text{obs}} = \tan^{-1}(d_{\text{obs}})^4, \quad (75)$$

where d_{obs} is the minimum distance from the drone’s global position to the nearest obstacle (which may be a boundary of the world) as found in the observation description below.

5) *Observations*: We provide the drone’s RL agent with an observation containing $3 + 3 + 3 + 24 = 33$ elements. The first (resp.) three are the drone’s velocity (resp. acceleration) in the global frame. The next three are the unit vector e_{goal} from the drone’s global position to the global goal. The last elements are the minimum distances to obstacles along 24 rays extending from the drone’s position (described below). If any of these distances are greater than 10 m, we set them to 10 m. So, one can write an observation for the drone as the tuple

$$o = (\dot{p}, \ddot{p}, e_{\text{goal}}, \{d_{\text{obs}}^{(i)}\}_{i=1}^{24}), \quad (76)$$

where each $d_{\text{obs}}^{(i)}$ is a distance along one of the 24 rays. The rays are created using spherical coordinates. We sample eight evenly-spaced azimuth angles in $[-\pi, \pi]$ rad, and use three elevation angles, at $-\pi/4$, 0 , and $\pi/4$ rad.